NUMERICAL STUDY OF TURBULENT BOUNDARY LAYER FLOWS OVER ROUGH SURFACES – PART II: TEMPERATURE PROFILES

Mila R. Avelino[*]
Department of Mechanical Engineering
University of Miami, Coral Gables, FL, USA
mila@uerj.br

Atila P. Silva Freire
Mechanical Engineering Program
Federal University of Rio de Janeiro – COPPE/UFRJ
Rio de Janeiro, RJ, Brazil
atila@serv.com.ufrj.br

Marcelo J.S. de Lemos
Departamento de Energia - IEME
Instituto Tecnológico de Aeronáutica - ITA
12228-900, São José dos Campos, SP, Brazil
delemos@mec.ita.br

Abstract. *Turbulent transfer of momentum and heat over rough surfaces are numerically simulated. The effects of sudden changes are predicted in the cases of turbulent flow around surface-mounted two-dimensional ribs when subjected to a sudden change in surface roughness and temperature. A particular interest of this study is to investigate the sudden changes in the surface roughness for developing thermal boundary layer flow. A two-equation k-eps turbulence model is employed to simulate the turbulent transport. Equations of boundary-layer type were used and a forward marching method was employed for sweeping the computational domain. Wall functions that take into account surface roughness are used to specify the boundary conditions at the surface. The effects of the sudden changes of roughness accounted for the wall functions in the k- eps turbulence model are compared with available experimental data. Four configurations are simulated here, namely one extensive uniformly smooth surface, one extensively uniform rough case, and two cases where the surface roughness varies suddenly from a smooth to a rough and from a rough to a smooth surface. Results are presented for velocity and skin friction coefficient, in addition to comparisons with experimental data. The use of a parabolic solver showed good agreement with experimental values for the mean and local quantities.*

Keywords. *Turbulent Flow, Numerical Study, Surface Roughness*

1. Introduction

One feature of the general turbulent heat transfer problem is that of fluids with low thermal conductivity, i.e., with Pr>1. In this case most of the resistance to heat transfer is concentrated in a thin layer near the wall, where it is difficult to conduct experimental measurements. The slightest errors in determining the transport mechanisms within the viscous layer and the fully turbulent region result in disagreement between analytic and experimental results.

The present work is concerned with flows that develop over flat surface with changing surface conditions. In particular, we will be looking at flows that present abrupt changes in surface roughness and temperature. The theory to be used here is, therefore, expected to account for these effects. Here, we will use the k-ε model to describe the properties of the boundary layer in the surface layer, and validated the results against the experimental data of Avelino (2000).

The k-ε model will use wall functions to represent the velocity and temperature profiles near the wall so that a local analytical solution for the inner region will be used as a boundary condition for the outer solution. This inner solution must take into account the local changes in the flow such as those caused by the changes on the surface roughness. Also, algebraic expressions that predict the sudden changes at the vicinities of the abrupt variation of the temperature and roughness conditions are applied. The local changes are then accounted for by logarithmic profiles that take as a characteristic length the displacement in origin, which has been experimentally studied by Avelino et al.(1998).

The present work is, therefore, to show the reader the influence of algebraic expressions that predict the sudden changes at the vicinities of the abrupt variation of the temperature and roughness conditions and how the k-ε model stands for flows over step changes in surface roughness and temperature if appropriate boundary conditions are made use of. Accordingly, the use of simple numerical tools for preliminary engineering design, instead of using memory-demanding, large Computational Fluid Dynamics (CFD) codes, can benefit the overall design process if repetitive calculations are mandatory. If no back flow is in order, marching-forward techniques, implemented along with isotropic turbulence models, provide an economical means for conceptual design using cheaper PC-based workstations.

Acknowledging the advantages of "fast" parabolic solvers, the work of Matsumoto e de Lemos (1990), presented results for the developing time-averaged and turbulent fields in a coaxial jet along a circular duct of constant area. Later, de Lemos & Milan (1997), extended their calculations to flow in long ducts through varying cross sections. Similar results for ducts with plane walls have also been documented in Braga & de Lemos (1999). The numerical methodology developed in all of that work is here employed. There, use was made of the isotropic k-ε model and the wall log-law for

---

[*] Reasearch Scholar from: State University of Rio de Janeiro, Mechanical Engineering Department, Rio de Janeiro, Brazil. Rua Sao Francisco Xavier, 524, suite 5023A.

velocity over smooth surfaces. Therefore, the present calculations used additional wall laws in order to account for rough walls.

2. Mean Flow and Turbulence

Next, the geometry investigated is detailed, followed by the governing equations, the numerical method used and the results obtained.

2.1. Geometry

The flow here analyzed consists of a confined stream inside a rectangular channel of constant cross section. Situations concerning surface roughness variation along the longitudinal coordinate are here considered. A schematic of the configuration under study is shown in Fig. 1. Four configurations were placed in the wind tunnel by alternating the position of the rough elements in the test section. The smooth surface was simulated as a reference case. In the other tree configurations, the roughness adopted was composed of transversally grooved surfaces with rectangular slats with height k=3mm, width s=12.0mm, and pitch λ=24.0mm.The grooves between the rough elements are 12mm wide (w=12.0mm).

It should be pointed out that mean velocity profiles are experimentally observed when the flow is subjected to sudden changes of the geometry conditions at the wall. In the vicinities of the abrupt change, the flow experiences a transition from one extensive region to another, being affected by the new geometry, until it reaches the fully rough regime. The theory used here does not represent the transition region, but the region where the flow has already reached the fully rough regime, where the numerical prediction shows good agreement with the experimental results.

2.2. Boundary Layer Equations

For generality, the equations below are written embracing planar and axi-symmetric cases. The equations are also presented in a simplified form, already making use of the concept of isotropic turbulent viscosity, μ_t.
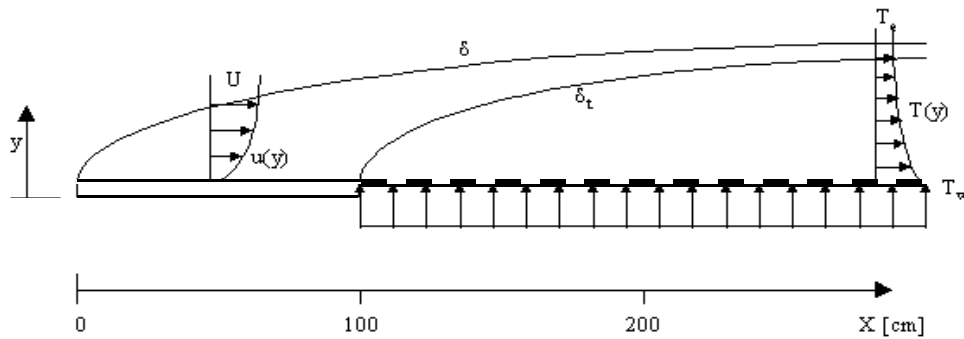
Fig. 1 – Test section and coordinate system for the smooth to rough surface.

$$\frac{\partial (r^\eta \rho u)}{\partial x} + \frac{\partial (r^\eta \rho v)}{\partial y} = 0 \quad , \tag{1}$$

$$\rho u \frac{\partial u}{\partial x} + \rho v \frac{\partial u}{\partial y} = - \frac{\partial p}{\partial x} + \frac{1}{r^\eta} \frac{\partial}{\partial y} \left[r^\eta \; \mu_{eff} \frac{\partial u}{\partial y} \right]. \tag{2}$$

Accordingly, the equations of continuity of mass and x-momentum for a two-dimensional, source-free, low speed, planar turbulent boundary (mixing) layer can be written as,

In (1)-(2) u, v are the velocity components in the axial and transverse direction, respectively, ρ the fluid density, p the static pressure, and μ_{eff} the effective (turbulent+laminar) coefficient of exchange given as, $\mu_{eff} = \mu + \mu_t$, where μ is the molecular viscosity. As mentioned before, equations (1)-(2) are written in a compact notation embracing planar (η=0) and axi-symmetric (η=1, r=y') cases. Further, in the k-ε model one has (Jones & Launder, 1972),

$$\mu_t = \rho \, c_\mu \, k^2 \, / \, \varepsilon , \tag{3}$$

where c_μ is a constant. Transport equations for k and ε are written as (Launder & Spalding, 1974),

$$\rho u \frac{\partial k}{\partial x} + \rho v \frac{\partial k}{\partial y} = \frac{1}{r^\eta} \frac{\partial}{\partial y}\left[r^\eta \ \Gamma_{eff}^k \ \frac{\partial k}{\partial y} \right] + S_k$$

$$\rho u \frac{\partial \varepsilon}{\partial x} + \rho v \frac{\partial \varepsilon}{\partial y} = \frac{1}{r^\eta} \frac{\partial}{\partial y}\left[r^\eta \ \Gamma_{eff}^\varepsilon \ \frac{\partial \varepsilon}{\partial y} \right] + S_\varepsilon$$

(4)

In (4), $\Gamma_{eff}^k = \mu + \mu_t/\sigma_k$ and $\Gamma_{eff}^\varepsilon = \mu + \mu_t/\sigma_\varepsilon$ where the Γ's are the effective coefficient of exchange and the σ's are the turbulent Prandtl/Schmidt numbers for k and ε. The last terms in (4) are known as "source" terms and are given by $S_k = \rho \, (P - \varepsilon)$ and $S_\varepsilon = \rho\varepsilon/k(c_1 P - c_2 \varepsilon)$ where c_1=1.47, c_2=1.92 and c_μ = 0.09. The production term reads

$$P = \frac{\mu_t}{\rho}\left(\frac{\partial u}{\partial y} \right)^2 .$$

(5)
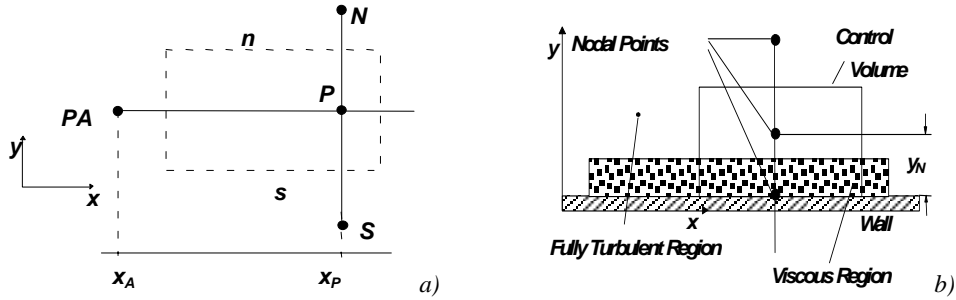
Fig. 2 – General notation for smooth wall model: *a*) Control volume, *b*) wall layer model.

2.3. Coordinate System

The numerical solution of Eqs. (1), (2) and (4) in the coordinate system _x-y_ presents some difficulties in regard to numerical precision. In this system, there is the disadvantage of having only a few nodal points where the boundary layer is "*thin*" and too many points where the thickness of the boundary layer has attained substantial growth. This work uses the coordinate system _x-ω_, proposed in Patankar (1988), by doing;

$$\omega = \frac{\Psi - \Psi_I}{\Psi_E - \Psi_I} .$$

(6)

where Ψ is the stream function and the subscripts I and E refer to the internal and external boundary layer limiting surfaces, respectively.

The equation set formed by (1)-(2)-(4) seen before can be written in the coordinate system _x-ω_ as (Patankar, 1988),

$$\frac{\partial \phi}{\partial x} + (a + b \ \omega)\frac{\partial \phi}{\partial \omega} = \frac{\partial}{\partial \omega}\left(c \ \frac{\partial \phi}{\partial \omega} \right) + d$$

(7)

where,

$$a = -\frac{d\Psi_I}{dx}/\Psi_{EI}; \qquad b = -\frac{d\Psi_{EI}}{dx}/\Psi_{EI}; \qquad c = r^2 \rho \ u \ \Gamma_{eff}^\phi \ /\Psi_{EI}^2 ;$$

$$d = S_\phi / (\rho u); \qquad \Psi_{EI} = \Psi_E - \Psi_I$$

(8)

In Eq. (7), ϕ can represent any of the dependent variables (ϕ =u,v,ε), Γ_{eff}^k is an effective coefficient of diffusion for ϕ and S_ϕ a source term. The discretization of (7) is obtained through the control volume method (Patankar & Spalding, 1972, Patankar, 1980) implying in (see Fig. 3a for notation),

$$a_P \phi_P = a_N \phi_N + a_S \phi_S + a_{PA} \phi_{PA} + b_P$$

(9)

where the coefficients involve convection, diffusion and source terms. For the solution of system (9) the Three Diagonal Matrix Algorithm is here adopted.

2.4. Inlet Conditions

Inlet flow is given a uniform distribution and the values of k and ε at entrance were assumed as,

$$k_{in} = C\, U_m^2, \quad \varepsilon_{in} = k_{in}^{3/2}/K\, y \tag{10}$$

where $C = {}^1\!/_2 Tu^2$, $Tu = \sqrt{3\overline{\left(u_i^{\,'}\right)^2}}\Big/U_m$ is the turbulence intensity at inlet, U_m is the overall mean velocity, K is the von Kármán constant (K=0.41) and y the distance to the wall. Halfway to the top surface (*y=H/2*) the symmetry condition is implemented for all dependent variables $\phi = u,k,\varepsilon$, as $\partial\phi/\partial y)_{y=0} = 0$.

2.5. Wall Treatment for Smooth Surfaces

The mathematical model seen above is not valid inside the layers very close to the wall where viscous effects are predominant. Velocity at the grid point closest to the wall is handled by the usual Wall Function approach described in Launder & Spalding (1972). The notation below refers to Fig. 3b where the location of the grid point closest to the wall, *N,* is identified. The wall function gives for the wall shear stress at node *N,*

$$\tau_w = \left(U_N\,\rho\, c_\mu^{1/4} k_N^{1/2}\right)\Bigg/ \frac{1}{K}\ln\left[E y_N \frac{\rho(c_\mu^{1/2} k_N)^{1/2}}{\mu}\right] \tag{11}$$

where E is a constant. In the wall region, the use of the wall function, characterized by the expressions,

$$U_N^+ = \frac{1}{K}\ln\left(y_N^+ E\right) \tag{12}$$

where

$$U_N^+ = \frac{u_N}{U^*}; \quad y_N^+ = \frac{\rho\, U^* y_N}{\mu}; \quad U^* = \sqrt{\frac{\tau_w}{\rho}} \tag{13}$$

and the employment of the assumption of "local equilibrium" for turbulence ($P=\varepsilon$), gives for point *N*,

$$k_N = \tau_w/(\rho c_\mu^{1/2}); \varepsilon_N = c_\mu^{3/4} k_N^{3/2}\Big/K\, y_N \tag{14}$$

2.6. Wall Treatment for Rough Surfaces

For rough surfaces, the equations above for the law of the wall are modified to take into account the effects for roughness. The basic facts about the laws of the wall for the velocity profiles have been discussed elsewhere (see Avelino et al. (1996)).

For computing the flow over the rough surface at the bottom of the wind tunnel, as shown in Fig. 1, Eq. (12) is modified for including the roughness function. Accordingly, an expression for the velocity profile valid for all types of roughness can be written if we make

$$\frac{u}{U^*} = \frac{1}{K}\ln\frac{(y_T + \in)U^*\rho}{\mu} + A - \frac{\Delta u}{U^*} \tag{15}$$

where,

$$\frac{\Delta u}{U^*} = \frac{1}{K}\ln\frac{\in U^*}{\nu} + C_i, \tag{16}$$

The domain of validity of (15)-(16) is the fully turbulent region and that can be verified through application of the single limit concept of Kaplun (1967) (see Silva Freire & Hirata, 1990).

In the above equations all symbols have their classical meaning; C_i, *i*= K, D is a constant characteristic of the type of roughness; the coordinate y_T is the distance measured from the crest of the roughness elements ($y = y_T + \in$); $\in$ is the displacement in origin, referred to in literature as the error in origin as well. Equations (15) and (16) will be used to specify the boundary conditions on a $k\text{-}\varepsilon$ formulation of the problem. The values for A, C_i and $\in$ used were 5.15, 4.3 and 1.9mm, respectively. Finally, rewriting (11) in the form $\tau_w = \lambda\mu(\partial U/\partial y)$ gives further,

$$\lambda = \begin{cases} 1 & \text{for laminar flow} \\[2em] \dfrac{K \, y_N \, \dfrac{\rho(c_\mu^{1/2} k_N)^{1/2}}{\mu}}{\ln\left[E \, y_N \, \dfrac{\rho(c_\mu^{1/2} k_N)^{1/2}}{\mu} \right]} & \text{for turbulent flow over smooth surface} \\[3em] \dfrac{K \, y_N \, \dfrac{\rho(c_\mu^{1/2} k_N)^{1/2}}{\mu}}{\ln\left[E_r \, \dfrac{y_N}{\in} \right]} & \text{for turbulent flow over rough surface} \end{cases} \tag{17}$$

2.7. The Displacement in Origin

The determination of the displacement in origin for the velocity profiles suggests that all the procedures advanced for the evaluation of $\in$ can be extended to the temperature profiles for the evaluation of $\in_t$. Thus, a straightforward extension of the method of Perry and Joubert(1963) to the temperature profiles can be made to evaluate $\in_t$, in the same way as for the velocity profiles.

The determination of the displacement in origin is significant for the evaluation of the properties of the flow over a rough surface, including all local and global parameters. All graphical methods for its determination, however, assume the existence of a logarithmic region, which may not occur near to a step change in roughness. The estimated values of $\in_t$ were obtained experimentally in Avelino(2000). In the numerical computations the expressions in Table 3 will be used to represent $\in_t$.
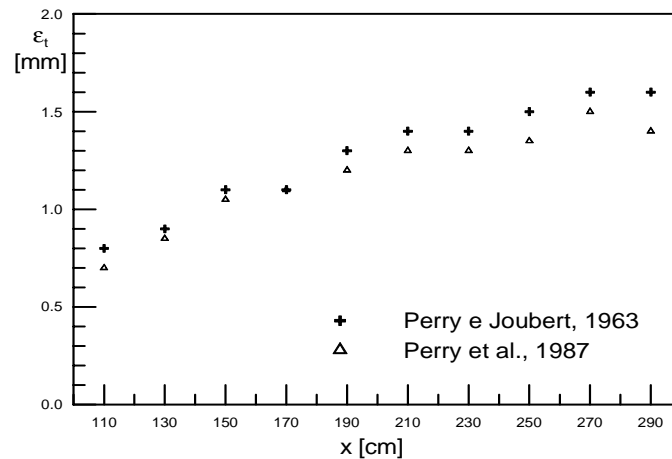
Figure 3. Displacement in origin for temperature profiles - Type I rough surface.

In the same way as for the velocity profiles, to determine the displacement in origin, the temperature profiles were plotted in semi-log form, in dimensional coordinates. Next, the normal distance from the wall was incremented by 0.1mm and a straight line fit was applied to the resulting points. Searching for the maximum coefficient of determination, the best fit was determined. Other statistical parameters were also observed, as the residual sum of squares and the residual mean square.

It is seen the experimental data agree with this analytical result for the smooth surface. Figures (3) and (4) present the evaluated temperature error in origin for all types of surfaces considered.

Table 1 – Estimated expressions for $\in_t$ obtained from the experimental data.

	Estimated expressions of $\in_t$	Estimated values for exponent 'm'
Surface Type I	$\in_t = 0.0013 \, x^m$	m=1.11
Surface Type II	$\in_t = 0.0121 \, x^m$	m=0.95
Surface Type III	$\in_t = 0.0180 \, x^m$	m=1.07
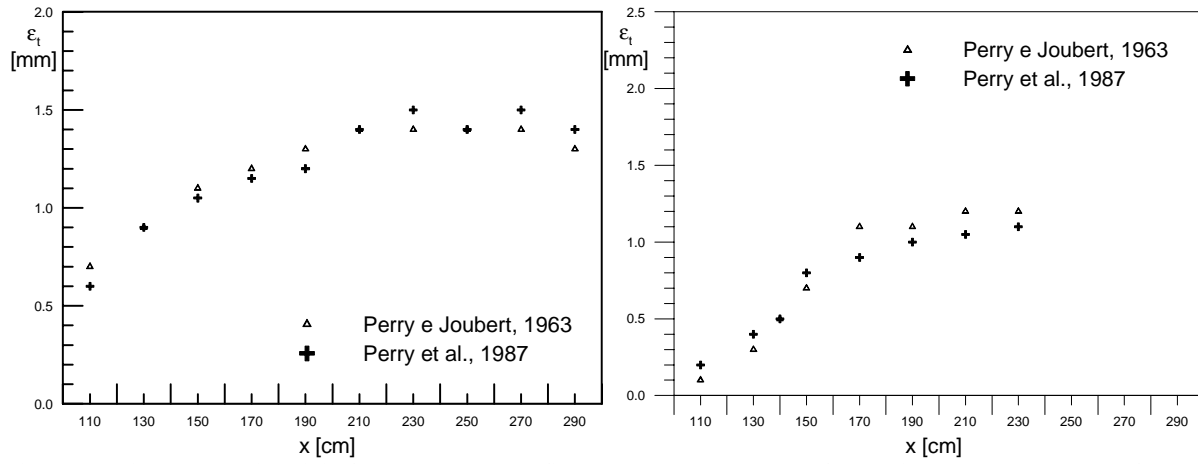
Figures 4. Displacement in origin for temperature profiles – (a) Type II rough surface and (b) Type III rough surface.

Expressions (15) and (16) can be extended to the thermal turbulent boundary layer through asymptotic or dimensional arguments. Based on similarity arguments for transfer processes in turbulent flows, Silva Freire and Hirata(1990) proposed to write the temperature law of the wall as

$$\frac{T - T_w}{t_\tau} = \frac{1}{k_t} \ln \frac{Pr(y_T + \in)u_\tau}{\nu} + B - \frac{\Delta T}{t_\tau} \qquad (20)$$

where,

$$\frac{\Delta T}{t_\tau} = \frac{1}{k_t} \ln \frac{Pr \in u_\tau}{\nu} + D_i \qquad (21)$$

and D_i, i= K, D; is a constant characteristic of the roughness.

Equations (20) and (21) are the law of the wall formulation for flows over rough surfaces with transfer of heat, and will be used to specify the boundary conditions on a k–ε formulation of the problem.

3. Numerical Algorithm and Computational Details

3.1. Pressure gradient

Determination of the unknown pressure gradient is handled as explained in Patankar (1988). That approach consists basically in finding the "zero" of a function $f(dp/dx)$ defined as;

$$f(dp/dx) = \left(A_{calc} - A_{duct} \right) / \Psi_{EI} \qquad (18)$$

where the left hand side represents the discrepancy, at the downstream position, between the calculated and real duct areas.

3.2. Integration step ($x_P - x_A$)

For the numerical solution of (9) at axial station x_P, the integration step size (x_P - x_A) determines the rate at which the longitudinal coordinate x is swept along the duct. In the vicinity of the boundary layer leading edge ($x\approx0$), the dependent variable ϕ (ϕ=u,v,$\mathcal{E}$,) varies more rapidly with x, if one considers the initial growth rate of the boundary layer. Therefore, the use of a small but constant value for (x_P - x_A) could be appropriate for the rapid changes of ϕ in the developing region but would imply in an excessive number of integration steps at the subsequent developed region. Likewise, a large value for (x_P - x_A) in the beginning of the sweep could, at the inlet region, cause numerical instability due to the large variation of all dependent variables within initial boundary layer development.

In this work, the integration step size was adopted as proportional to the distance from the point in question to the beginning of the calculation as:

$$\frac{x_P - x_A}{H} = \left[\frac{x - x_I}{x_L - x_I} \right]^\beta \qquad (19)$$

where indexes "I" and "L" correspond to the initial and final x positions, respectively, H is one half of channel height and β is a constant.

3.3. Transversal distribution of nodal points

In the boundary layer close to the duct wall the discretization of the production term for k, Eq. (5), is rather sensitive to the transverse grid layout. A flexible grid point distribution is obtained by the use of a coordinate transformation of the type $\phi = (y')^{\alpha}$, giving for discrete positions along the transversal coordinate,

$$y_i = \left(\frac{R^{\alpha}}{N} - y_{i-1} \right)^{1/\alpha} \tag{20}$$

where "i" in (20) is the index of the nodal point in question and α a parameter for grid control.

4. Results and Discussion

Numerical results calculated with the model shown above were used to simulate the flow over the flat surface of Fig. 1. Four cases were investigated and classified according to the relative smooth-to-rough length section. Computations used different wall boundary conditions, based on Eq. (17), which were applied over the corresponding surface length detailed in Table 2. The results to follow were compared with measurements of Avelino et al. (1999).

Table 2 – Length of smooth and rough sections for the cases investigated

Case	Smooth Surface	Rough Surface
Fully Smooth	0m< x < 2m	-
Smooth to Rough	0m< x < 1m	1m< x < 2m
Fully Rough	-	0m< x < 2m
Rough to Smooth	1m< x < 2m	0m< x < 1m

Figures 4 to 7 show comparisons of T^+ versus y/δ, where δ is the boundary layer thickness, for the four different cases presented in Table 2. Profiles at fifteen longitudinal stations are compared with the numerical prediction showing good agreement. The lines represent the numerical predictions whereas experimental values are plotted with symbols.

Profiles here calculated at stations in the vicinity of the surface conditions variation, for T^+ did not quite match those of the experimental dada, most likely due to the transition region explained earlier. In this work the value of the displacement in origin was assumed constant, although it adjusts itself when over a new rough geometry.

The interesting feature of Figs. 5 to 7 is that in spite of using a parabolic solver and a linear k-ε model, the present calculation seems to represent quite well the phenomena.

Here, based on the results shown, it is suggested that, for accurate flow prediction, an expression representing the increase in $\in$ should be implemented, to better predict the development of the boundary layer immediately after the changes in the wall roughness. In other words, a function of a characteristic length scale of the rough elements can be used for the prediction of the velocity profiles in the transition region of the flow.

After observing Figs. 5 and 6, the overall conclusion is that for the smooth surface, and in the region upstream of a step change in roughness, the numerical prediction seem to agree reasonably well with the experimental results, however, in the transition region of the boundary layer flow, a small discrepancy can be observed close to the wall. Those differences are likely due to the gradual growth of the displacement in origin, until it reaches a constant value, where the velocity profiles are then accurately predicted.

Corresponding skin friction coefficient values are shown in Figs. 8 to 11. In these figures, numerical prediction is compared with those calculated through an integral method and a graphical determination, based on the experimental results. For the case of a uniformly smooth surface, a theoretical correlation is also included.

The nature of the variation of the temperature profile that is a function of Pr is quite important. The effect of properties variations on the velocity profile for opposite directions of heat flux is different. This is also related to the nature of variation in the temperature profile. If air is heated by the plate, its viscosity and thus the Pr at the wall will increase.

It is clear from Fig. 8 that the numerical prediction is in good agreement with the theoretical correlation for turbulent boundary layers over smooth surface, and with the experimental results, either calculated by using the integral balance of the momentum or through the chart method.

It can be noticed in Figs. 9 and 10, where the step change in roughness are present that the numerical prediction responds very fast to the new surface condition. In Fig. 9, the displacement in origin presents an increase following the step change in roughness, increasing the skin friction coefficient, what is expected for the flow over a rough surface. This effect is well captured by the numerical model. Also the momentum balance and the graphical method are in good agreement.

For the configuration where the flow leaves a rough surface, to come upon a smooth surface, Fig. 10, a departure from experimental values can be observed immediately after the sudden change in the roughness. This fact is due to the transition region that the flow undergoes following the surface step change.
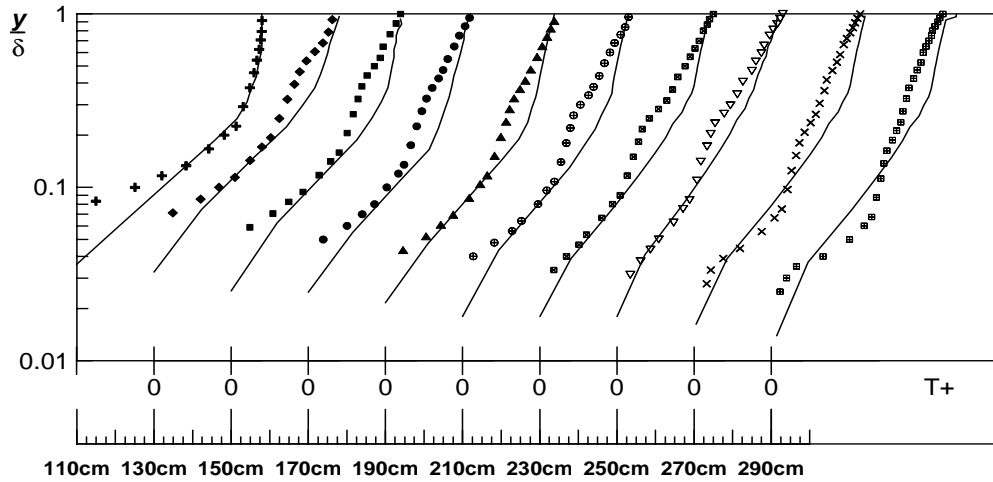
Fig. 5 – Mean temperature over rough surface type I, comparison with experimental results.
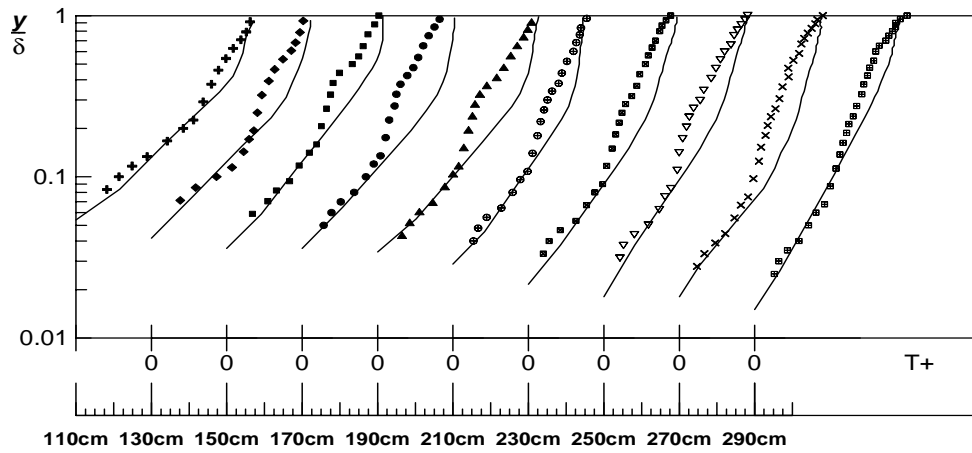
Fig. 6 – Mean temperature profiles over rough surface type II, comparison with experimental results.
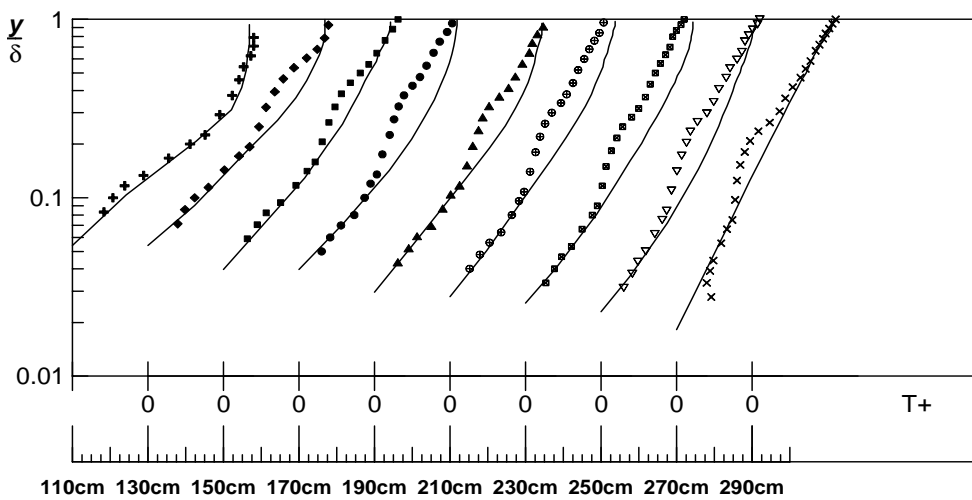
Fig. 7 – Mean temperature profiles over rough surface type III, comparison with experimental results.

When in contact with a smooth surface, the displacement in origin tends to decrease until it vanishes, and this can be noticed by either the integral method or by the chart method, conversely, in the parabolic solver, this effect cannot be caught. In fact, in the numerical model above, no mechanism that could bring back information from downstream positions is considered. The flow, in this case, can be characterized as of partially parabolic nature requiring an elliptic solver for the pressure field.
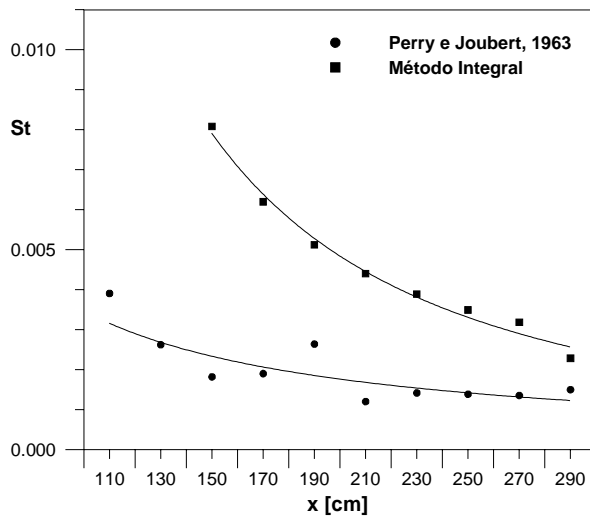
Fig. 8 – St Number prediction over smooth surface.   Fig. 9 – St Number prediction over rough surface type II.
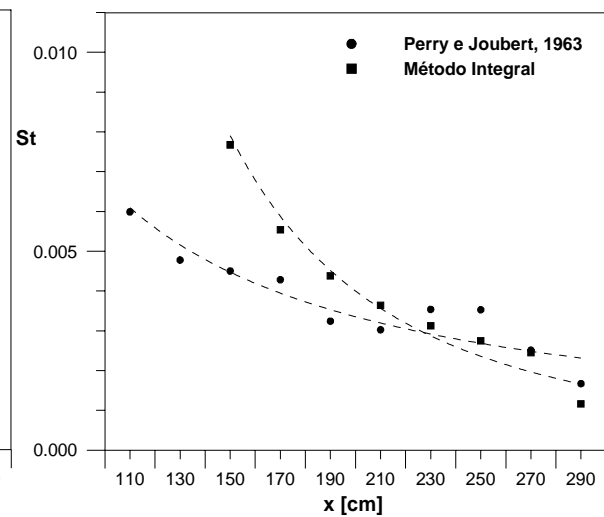
For engineering purposes, however, the parabolic treatment has proven to be adequate for reproducing the major features of the flow.

These results are coherent with the idea of limiting the present model to the regions of the flow where the displacement in origin has already reached a constant value, in the fully rough region of the flow.

The determination of the displacement in origin, $\in$, is crucial for the evaluation of the properties of the flow over a rough surface, including all local and global parameters such as, e.g., the skin-friction coefficient and the momentum thickness. All graphical methods for its determination, however, assume the existence of a logarithmic region, which may not occur near to a step change in roughness.

5. Concluding Remarks

This work presented computations with the standard k - ε model for simulation of turbulent boundary layer flows that present abrupt changes in the surface roughness.

Comparisons with experimental data indicated a reasonable agreement. More specifically, for surfaces subjected to sudden changes in roughness, demonstrated that the methodology here employed gave better or comparable results than those calculated with more sophisticated numerical tools and employing more elaborated turbulence modes. Accuracy of the calculated skin friction coefficient is also limited in the region where the displacement in origin is still adjusting itself to the new surface.

Essentially, the work herein suggests that, for accurate prediction of simple flows, proper implementation of the numerical model and the robustness and stability of the algorithm employed are important factors to be considered. Accordingly, for boundary layer flows, isotropic turbulence theories and simple parabolic codes can provide an economical and reliable tool during preliminary steps in the overall design process of engineering equipment.

6. Acknowledgement

7. References
Avelino, M.R., 1996, Sobre a Modelagem Diferencial de Camadas Limite Turbulentas com Transpiração, Msc. Thesis, PEM/COPPE/UFRJ.
Avelino, M.R., 2000, An Experimental/Numerical Study of the Turbulent Boundary Layer Development along a Surface with a Sudden Change in Roughness, *J. of Braz. Soc. Mechanical Sciences*, Vol. XXII, No. 1, pp. 1-13.

Avelino, M.R., Menut, P.P.M., Silva Freire, A.P., 1998. Experimental Characterization of a Turbulent Boundary Layer Subjected to a Step Change in Surface Roughness, *Proc. of 3rd Braz. Therm. Sci. Meet.* , Vol. II, pp. 1369-1374, Rio de Janeiro, RJ, Brazil.

Avelino, M.R., Menut, P.P.M., Silva Freire, A.P., 1999, Characteristics of the Turbulent Boundary Layer Over Surfaces with Abrupt Variation in Properties, *Trends Heat Mass Transf.*, Vol. 5, pp. 63-80.

Avelino, M.R., Kakac, S., and de Lemos, M.J.S., 2001, Numerical Study Of Turbulent Flow Subjected To Sudden Changes In Wall Roughness *Proc. of COBEM02- 14th. Braz. Congr. Mech. Eng*, Uberlandia, Brazil, Nov. 22-26.

Braga, E.J., de Lemos, M.J.S., 1999, Numerical Analysis of Coaxial Turbulent Jets in Diffusers and Contractions, *Proc. of COBEM99- 13th. Braz. Congr. Mech. Eng.*, Águas de Lindóia, SP, Brazil, Nov. 22-26.

de Lemos, M.J.S., Milan, A., 1997, Mixing of Confined Coaxial Turbulent Jets in Ducts of Varying Cross Section, *Proc. of COBEM97 - 12$^{th.}$ Braz. Cong. Mech Eng*., Bauru, São Paulo, Brazil, December 8-12.

Jones, W.P., Launder, B.E., 1972, The Prediction of Laminarization with a Two-Equation Model of Turbulence, *Int. J. Heat & Mass Transfer*, vol. 15, pp. 301-314.

Kaplun, S., 1967, Fluid Mechanics and Singular Perturbations, Academic Press.

Launder, B.E., Spalding, D.B., 1972, Lectures in Mathematical Models of Turbulence, Academic Press, New York.

Launder, B.E., Spalding, D.B., 1974, The Numerical Computation of Turbulent Flows, *Comp. Math. App. Mech. Eng.*, vol. 3, pp. 269-289.

Matsumoto, E., de Lemos, M.J.S., 1990, Development of an Axi-Symmetric Mixing Layer in A Duct of Constant Cross Section, *Proc. of 3rd Braz. Therm. Sci. Meet.*, vol. I, pp. 381-385, Itapema, Brazil, December 10-12.

Patankar, S.V., 1980, Numerical Heat Transfer and Fluid Flow, Mc-Graw Hill.

Patankar, S.V., 1988, Parabolic Systems, Chapter 2 of Handbook of Numerical Heat Transfer, Rohsenow *et al* Ed., John Wiley & Sons, NY.

Patankar, S.V., Spalding, D.B., 1972, A Calculation Procedure for Heat, Mass and Momentum Transfer in Three-Dimensional Parabolic Flows, *Int. J. Heat & Mass Transf.,* vol. 15, pp. 1787-1806.

Perry, A.E. e Joubert, P.N., 1963. Rough-Wall Boundary Layers in Adverse Pressure Gradients, J. Fluid Mech., Vol. 17, pp. 193--211.

Silva Freire, A.P., Hirata, M.H., 1990. Analysis of Thermal Turbulent Boundary Layers over Rough Surfaces, Proc. *Proc. of 3rd Braz. Therm. Sci. Meet.*, vol. I, pp. 381-385, Itapema, Brazil